Numerical Modeling of a Church Nave Wall Subjected to Differential Settlements: Soil-Structure Interaction, Time-Dependence and Sensitivity Analysis

Anastasios Drougkas[1]

Building Materials and Building Technology Division, Civil Engineering Department, KU Leuven, Kasteelpark Arenberg 40 Box 2448, B-3001 Heverlee, Belgium

Els Verstrynge

Building Materials and Building Technology Division, Civil Engineering Department, KU Leuven, Kasteelpark Arenberg 40 Box 2448, B-3001 Heverlee, Belgium

Pepijn Szekér

Building Materials and Building Technology Division, Civil Engineering Department, KU Leuven, Kasteelpark Arenberg 40 Box 2448, B-3001 Heverlee, Belgium

Gert Heirman

Triconsult nv, Lindekensveld 5 box 3.2, B-3560 Lummen, Belgium

Leidy-Elvira Bejarano-Urrego

Building Materials and Building Technology Division, Civil Engineering Department, KU Leuven, Kasteelpark Arenberg 40 Box 2448, B-3001 Heverlee, Belgium

[1] Corresponding author, email: anastasios.drougkas@kuleuven.be

Giorgia Giardina

Department of Architecture and Civil Engineering, University of Bath, Claverton Down, Bath, BA2 7AY, United Kingdom

Koenraad Van Balen

Building Materials and Building Technology Division, Civil Engineering Department, KU Leuven, Kasteelpark Arenberg 40 Box 2448, B-3001 Heverlee, Belgium

Abstract

Historic masonry structures are particularly sensitive to differential soil settlements. These settlements may be caused by deformable soil, shallow or inadequate foundation, structural additions in the building and changes in the underground water table due to the large-scale land use change in urban areas.

This paper deals with the numerical modeling of a church nave wall subjected to differential settlement caused by a combination of the above factors. The building in question, the church of Saint Jacob in Leuven, has suffered extensive damage caused by centuries-long settlement. A numerical simulation campaign is carried out in order to reproduce and interpret the cracking damage observed in the building.

The numerical analyses are based on material and soil property determination, the monitoring of settlement in the church over an extended period of time and soil-structure interaction. A sensitivity study is carried out, focused on the effect of material parameters on the response in terms of settlement magnitude and crack width and extent. Soil consolidation over time is considered through an analytical approach. The numerical results are compared with the in-situ observed damage and with an analytical damage prediction model.

Keywords

Masonry; soil-structure interaction; historic structures; finite element modeling; settlement-induced damage

Highlights

- A masonry church nave wall subjected to differential settlements is numerically modeled, considering time-dependent material properties combined with changes in geometry and loading
- The foundation and the soil properties are directly considered
- A sensitivity analysis highlights the parameters affecting the cracking pattern and extent
- The phased analysis results in a much more accurate representation of the observed damage compared to a single-phase model
- An analytical model for the calculation of damage due to differential settlements is expanded and compared to the finite element analysis results

Notation

E	Young's modulus
G	shear modulus
ν	Poisson's ratio
ρ	mass density
σ_t	tensile stress
ε_{cr}	crack strain
ε_u	ultimate strain
f_c	compressive strength
f_t	tensile strength
G_f	tensile fracture energy

h	characteristic finite element length
L^j	footing half-length
B^j	footing half-width
D^j	footing embedment depth
A_f^j	footing area
A_w^j	footing side-wall contact area
K_n^j	footing vertical elastic stiffness
k_n^j	footing modulus of subgrade reaction
k_n	wall/colonnade modulus of subgrade reaction

1. Introduction

1.1 State of the Art

The analysis of large monumental structures subjected to differential ground movement is a challenging subject of study. The challenge mainly arises from geometric complexity and sheer size, problems only partially mitigated by a detailed geometric survey, material property determination and the definition of the applied deformation load profile through concerted monitoring efforts [1]. It is, however, a worthwhile endeavor in service of estimating the risk of damage or collapse and designing effective intervention strategies for repair and strengthening.

The discretization of monumental church structures in macro-elements with different stiffness is often considered conceptually and empirically valid. Macro-elements, such as façades, towers, apses and single naves, are often separated through insufficient tying and the presence of structural cracking. They are further

characterized by different stiffness, weight and internal stresses. Namely, the effects of earthquake action and differential settlement loading affect different parts of the structure in distinct ways. Therefore, the problem of structural analysis of large churches can be simplified by pursuing it on an individual macro-element basis [2]. It is both practical and valid to study certain components of monumental church structures, such as single bays, naves, façades or towers individually.

In a nonlinear finite element (FE) analysis framework, the large dimensions of monumental church structures built in masonry can render detailed modeling computationally prohibitive and model preparation effort excessive. As an alternative to nonlinear FE modeling, rigid block analysis has been shown to be capable of reproducing failure modes in masonry structures subjected to large movement of their supports [3,4]. When failure is mostly concentrated in the joints, either through sliding and/or opening, as is the case in dry joint masonry and, usually, in masonry with weak lime mortar joints, rigid block analysis becomes an attractive approach. However, sheer size and geometrical complexity, due to an irregular bond and the existence of multiple masonry leaves, render such approaches difficult to implement in large structures. Macro-modeling, therefore, which consists in the homogenous modeling of the masonry composite, becomes a more suitable alternative. Despite the assumption of homogeneity, nonlinear macro-modeling of large masonry structures can provide insight into the mechanisms through which damage arises and expands [5,6].

Predictive models for damage estimation and categorization in masonry structures subjected to differential ground movement have been proposed in the literature [7–9]. These models rely on the determination of parameters related to the material, geometric and foundation properties of the structure and are mostly used to evaluate the effects of tunneling-induced settlements. The loading parameters for these models can be determined using terrestrial or space-borne means, comparing the differential settlement to empirical, semi-empirical or calculated limits for the determination of the level of damage. The analytical and parametric basis of these models allows their adoption and modification according to the requirements of a variety of loading scenarios and foundation types. The application spectrum of such methods extends from damage prediction in individual

buildings to vulnerability assessment in entire urban aggregates. This basis further allows the parallel application with, and direct comparison to, numerical modeling of damage induced by differential ground settlement.

In this paper both numerical and analytical models are applied for the analysis of a large monumental structure. The church of Saint Jacob in Leuven has been the subject of wide and inclusive study over the preceding decades [10–12]. It is characterized by extensive and developing damage due to differential ground movement. This damage is well documented and extensive data is available on the profile of ground movement over different periods. Finally, studies have been performed on its material properties, the stress state of its structural elements and the properties of the foundation soil. It is therefore a prime candidate for investigation through analytical simulation and numerical analysis for the purpose of interpreting the damages present in the fabric and the development of ground movement.

1.2 Objectives

The focus of the present paper is the numerical reproduction of the damage patterns observed over time in the church of Saint Jacob in Leuven, the investigation of their underlying cause, namely the differential settlements at the site, and the study of the effect of material and numerical analysis parameters in the obtained results. This is accomplished through a sensitivity study involving the material properties of the masonry structure, the application of different loading patterns in the form of settlement profiles and the variation of the boundary conditions as affected by the passage of time.

The interpretation of the results of the numerical analyses, coupled with the assembly and evaluation of historic data, on-site observations and structural monitoring aim at providing insight into the occurrence and development of structural damage in the monument. A quantitative assessment of the development in time of soil consolidation under the effect of gravity loads is given, thus outlining the behavior of the monument over an extended period.

Further interpretation and quantification of the numerical results is provided through their comparison with simplified analytical damage assessment models. This comparison allows the evaluation of the applicability of

analytical models in monumental masonry structures and demonstrates their potential for the interpretation of current and the prediction of future structural damage.

2. The Case Study

2.1 Layout and Brief Historic Outline

Details on the history of the construction of the church may be found in [10], with the main points repeated here for clarity. Construction of St. Jacob's church began around 1220, with the erection of the tower over the remnants of an existing Romanesque church. The initial plan called for the church to have a flat timber ceiling, which was later substituted for a timber barrel vault. The main nave, at its originally intended height, was completed in the 14th century, along with the side naves and their stone vaults, and the bell tower over the crossing was added in the 15th. During the period 1534-1535, an additional level over the main nave was added and masonry vaults were added in place of the timber vault, which was complemented by the addition of two, possibly four, pairs of flying buttresses. These alterations resulted in the addition of self-weight not originally anticipated in the construction of the foundations.

First mention of structural problems stemming from differential settlement dates back to at least the 15th century. These problems led to the reconstruction of the side nave vaults. The timber bell tower over the crossing was dismantled in 1735 due to concerns over its decay. The development of vertical cracking in the pillars led to the installment of confining steel rings in the early 19th century, still present. Further consolidation measures were taken in the early 20th century due to severe cracking in the west wall of the northern transept. In 1963, the entire church was definitively closed for the public. During the partially executed consolidation works of 1965-1971, the structure was internally shored using massive reinforced concrete elements and steel profile braces. While only foreseen as a temporary measure, the shoring members are still present today. Additionally, the side nave vaults were dismantled for weight reduction. In 2000 the flying buttresses were removed due to their being severely out-of-plumb, which raised concerns of sudden collapse, and were replaced by temporary steel tie-rods. A comprehensive structural intervention project, including localized repairs on the masonry a micro-piling

reinforcement of the foundations and reconstruction of the dismantled elements (side nave vaults and flying buttresses) and soil consolidation was launched in September 2018 [13].

A floor plan of the church, along with the designation of the construction phases, can be seen in Figure 1. The construction process, beginning with the tower and following with the arcade, naves, transept, chapels and finally the choir are indicated.

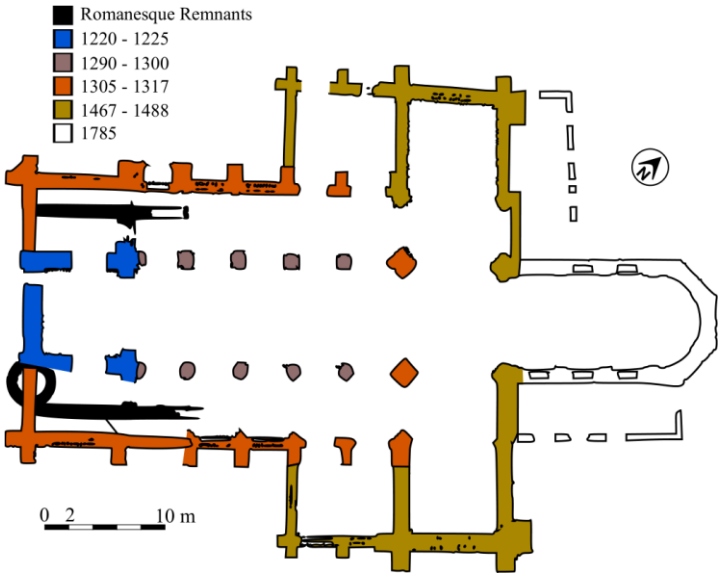

Figure 1 Church floor plan and construction phases. Adapted from [10]**.**

2.2 Damage Survey

The differential settlements in the church, which are the cause of the clear majority of structural damage, are caused by the building being erected in a swamp area near the river Voer, coupled with the initially unplanned addition of a second and third level, resulting in a severe increase in self-weight. The substitution of the original flat timber ceiling with a wooden barrel vault and, later, a masonry vault resulted in further increase in the self-weight.

The present study focuses on the damage documented in the northern wall of the main nave. An elevation view, the main structural elements and damage, along with the notation used for their designation, is shown in Figure 2. The nave wall measures approximately 26 m in length and 21 m in height. The damage of the nave,

consisting primarily of cracks caused by differential settlement, has been documented both with hand drawings and photographically during site visits, and more recently using semi-automated point-cloud data processing [14].

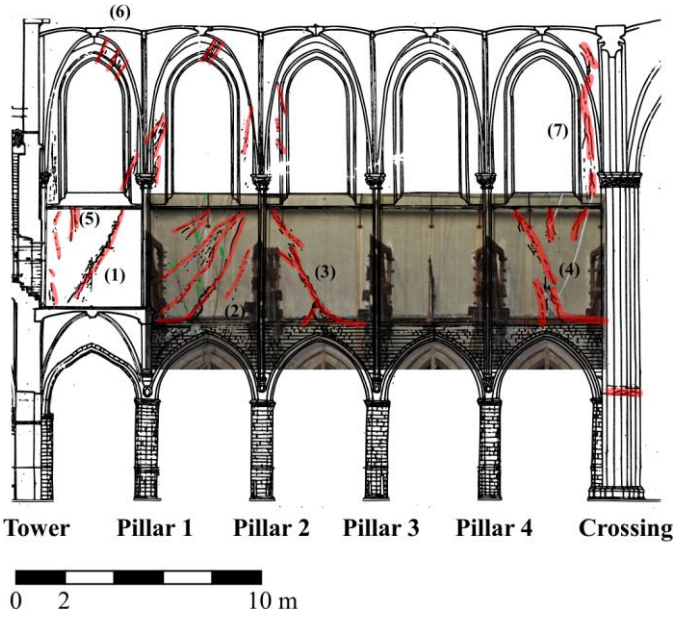

Figure 2 Northern wall of main nave: structural element designation and documented major cracks indicated in red (adapted from a hand-drawn survey of the building's geometry and pathology carried out by students of the Raymond Lemaire International Centre for Conservation, 1983-1984 [15]**). In underlay a photographic survey of northern nave wall cracks. View of cracks above nave pillars (photo by Pepijn Szekér, 2018).**

The arithmetically designated cracks 2 through 4 of the nave have been photographically documented and are shown in underlay in Figure 2. Continuous visibility of cracks 1 through 4 is not possible due to the obstruction caused by the organ loft near the western tower. Despite the time passed between the survey in 1983-1984 and the photographic survey in 2018 (Figure 2), there does not appear to be any lengthening of the major cracks. However, the same cannot be said with certainty about the crack widths, however, since these were not measured in the prior case.

The widths of the cracks above the nave pillars have been measured by hand. While the external plaster presents a crack width of a few mm, the crack width on the masonry behind the plaster is roughly between 10mm

and 20mm (i.e. eroded mortar joints), Figure 3. The cracks appear to mostly pass through the mortar joints rather than splitting the masonry stone units in the investigated area.

Figure 3 Close-up of cracks 4 on main nave wall (photo by Els Verstrynge, 2018).

2.3 History of Settlements: Estimation and Geomatic Data Processing

An estimation of the soil settlements for different parts of the structure, under different calculated loads, has been carried out in the extensive studies of the church. These results are presented in internal technical reports, property of KU Leuven [15]. These settlements are presented for the tower, crossing and pillars in Figure 4 and have been calculated based on cone penetration tests and evaluation of the soil consolidation progress according to Terzaghi, Buisman and Koppejan [16]. The results are not differentiated between individual pillars, thus rendering the calculation of the differential settlement between pillars impossible. Since the tower was completed before the beginning of the construction of the nave, an additional graph of the development of the tower settlement is provided. This graph ignores the settlements occurred before the completion of the nave wall (see grey line in Figure 4).

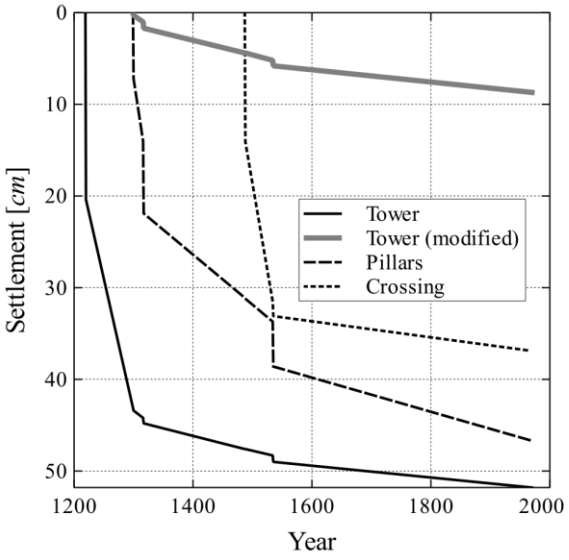

196

197 **Figure 4 Calculated settlements for different structural components of the tower and nave from 1220**
198 **to 1970 (adapted from** [15]**).**

199 Concerning more recent ground movement and the resulting differential settlement of the pillars, levelling
200 surveys conducted over the previous two decades provide info on the development of differential settlements over
201 selected periods of measurements. Contour plots of the settlements over the period 1994-2005 are presented in
202 Figure 5. These geodetic survey results are presented in terms of settlement relative to a point in the choir which
203 is considered, due to the absence of apparent damage, stable. The maximum settlement over this period was
204 measured at the area around pillars 1 and 2 of the northern nave, with areas at the southern nave and northern
205 transept presenting some uplifting. The settlement at pillars 1 and 2 is consistent with cracks 1, 2 and 3 as indicated
206 in Figure 2, although the time of the first appearance of these cracks is not known with certainty. It is interesting
207 to note that all points along the nave exhibited a rather uniform settlement in the period 1994-2000, while in the
208 period 2000-2005 the settlement of pillar 2 appeared to increase at a faster rate than the other points in the nave.

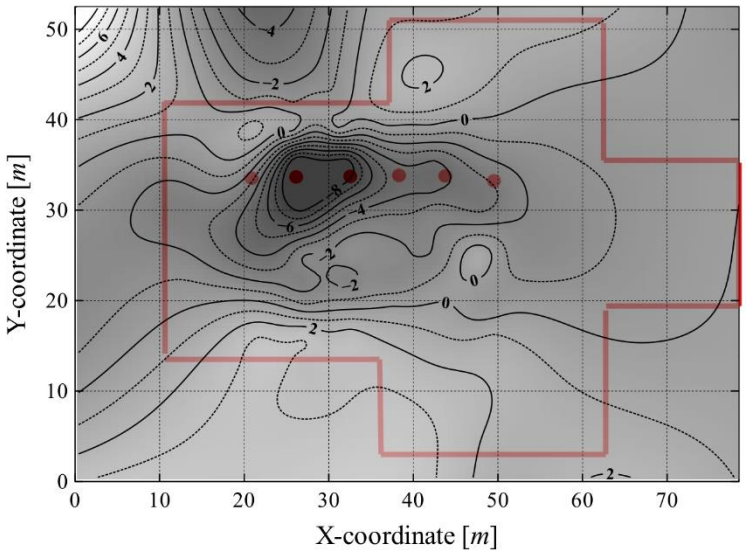

Figure 5 Contour plot of ground settlement in mm during the period 1994-2005 against church architectural outline. Location of northern nave from tower pilaster to crossing indicated by solid hatch circles.

An additional third approach may be adopted for the evaluation of the differential settlements over the entire history of the church. This is accomplished through the study of the geometric disposition of characteristic architectural features present on the structural elements. This approach is based on detailed laser scanning data acquired in the context of this investigation [14]. The downside of this rough approach is the inability to evaluate the total settlement that each element has undergone: only the final differential settlement can be estimated. Five reference features are chosen for this approach, from top to bottom: 1) the top of the third level arches' voussoirs, 2) the base of the pilaster abacus of the third level, 3) the top of the first level arches' voussoirs, 4) the base of the pillar abacus of the first level and 5) the top of the first level pillar pedestals. Assuming that features 1-2, and similarly 3-4-5, were built at the same period, it follows that they were, in all probability, vertically level at the time of construction.

The measured vertical displacements relative to pillar 1 (lines 2, 4-5) or arch 2 (lines 1, 3) are shown in Figure 6. All architectural features are present in pillar 1 and its neighboring arch span, hence the choice of these elements as a reference, instead of, for example, the crossing column. The obtained profile is similar to the profile found in

the recent leveling measurements, with the settlement being mostly concentrated around pillars 1 and 2. This is consistent with the formation of cracks 2 and 3 (Figure 2). Differences in the profile at different heights of the structure are expected for two reasons: a) differential settlement generally affects the lower parts of the building more severely and b) the second and third levels of the nave wall were constructed at a later phase, when part of the settlements of the colonnade had already occurred.

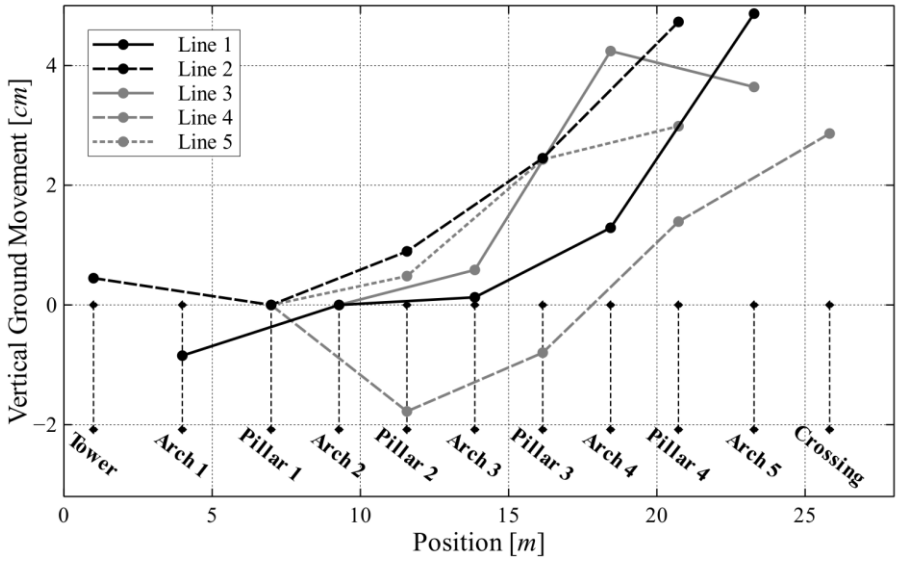

Figure 6 Differential settlements relative to pillar 1 (position: 6.99 m) measured from point cloud data architectural feature analysis. Position distance measured from tower pilaster.

3. Analysis Procedure

3.1 Modeling the Nave Wall

The geometry of the nave is derived from an idealization of the in-situ geometry in its undeformed state. A distinction is made between the three-leaf masonry of the nave wall and the solid stone masonry of the lower part of the pillars, each with its own set of material properties. The basic values of the material properties used for the numerical analyses, in part determined in previous experimental efforts [10,11] and in part assigned nominal or empirical values as proposed in the relevant literature [17,18], are summarized in Table 1.

Table 1 Basic material properties used in numerical analysis.

	E $[N/mm^2]$	ν $[-]$	ρ $[kg/m^3]$	f_c $[N/mm^2]$	f_t $[N/mm^2]$	G_f $[N/mm]$
Wall masonry	3000[c]	0.15[c]	**1920**[b]	**6.99**[a]	0.10[c]	0.012[d]
Pillar masonry	**15700**[b]	**0.20**[b]	**2360**[b]	**11.95**[a]	1.00[d]	0.075[d]

a: experimentally derived value [10]
b: experimentally derived value [11]
c: estimated value [17]
d: estimated value [18]

The masonry walls and columns of the nave are modeled using 8-node quadrilateral and 6-node triangular plane stress elements, an approach suited to the geometric arrangement, element thickness and load orientation. A macro-modeling approach is adopted for the model, in which the masonry composite is treated as a homogenous continuum, with no distinction between units, mortar and the unit-mortar interface. The nonlinearity in tension is modeled using a multi-directional fixed crack model [19]. The model is based on a decomposition of the total tensile strain into an elastic and a crack component. The crack strain is further decomposed, allowing for the formation of a number of cracks simultaneously. A Rankine-type tension cut-off is used in pure or biaxial tension, while the influence of lateral compression is accounted for through a Mohr-Coulomb-type criterion. Nonlinear tension softening is assumed, governed by fracture energy, according to the expression:

$$\sigma_t = \begin{cases} f_t\left(1 - \dfrac{\varepsilon_{cr}}{\varepsilon_u}\right)^{0.31} & for \quad 0 \le \varepsilon_{cr} \le \varepsilon_u \\ 0 & for \quad \varepsilon_u \le \varepsilon_{cr} < \infty \end{cases} \tag{1}$$

where σ_t is the tensile stress, ε_{cr} is the crack strain and ε_u is the ultimate strain, calculated according to the expression [20]:

$$\varepsilon_u = 4.226\frac{G_f}{f_t h} \tag{2}$$

where h is the characteristic length of the finite element. The fracture energy/characteristic length approach results in mesh objectivity, provided the element length is sufficiently small to avoid a constitutive snap-back. The

maximum size criterion, based on the requirement for the initial tangent of the tensioning softening diagram to be less than the Young's modulus, is satisfied for the chosen element length.

While the nave cracks appear to be mostly developed along the joints and not through the units. A detailed modeling approach based on rigid-block or block-joint models could potentially be employed. However, the dimensions of the structure are prohibitive for such detail to be practical. The geometric survey would need to include detailed information on the dimension and arrangement of the outer leaf stones. Further, even if nominal dimensions and a regular pattern were adopted, the infill would still need to be individually modeled. Macro-modeling was therefore adopted as a practical solution, nevertheless capable of providing sufficiently detailed results for the purposes of the paper.

The steel rings installed in the 19th century were not included due to the lack of data on their material properties and state of decay. It is not expected, however, that this omission affects the cracking of the nave walls to any significant extent.

3.2 Foundation and Soil-Structure Interaction

Soil-structure interaction is directly considered through the introduction of linear elastic structural interfaces at the base of the masonry pillars, capable of accounting for normal and shear deformation. The normal stiffness may be determined according to two distinct approaches: (a) from a calibration effort targeted at reproducing the settlement profile measured over a given time period and (b) directly from the geometric characteristics of the pillar footing and the elastic properties of the soil.

Both approaches are adopted and compared in the present paper. The values obtained from approach (a) are presented in the results section. For approach (b), the vertical elastic spring constant for a single rigid arbitrarily shaped footing j circumscribed in a rectangle with dimensions $2L^j \cdot 2B^j$ and embedded in the ground at a depth of D^j is equal to [21]:

$$K_n^j = \frac{2GL^j}{1-\nu}(0.73 + 1.54x^{0.75})\left[1 + \frac{1}{21}\frac{D^j}{B^j}(1 + 1.3x)\right]\left[1 + 0.2\left(\frac{A_w^j}{A_f^j}\right)^{2/3}\right] \quad (3)$$

where G is the shear modulus of the soil, ν is the Poisson's ratio of the soil, A_f^j is the area of the footing, A_w^j is the total sidewall-soil contact area (equal to the perimeter of the footing times the embedment depth D^j in case of a foundation with constant cross-section) and $x = A_f^j/\left(2L^j\right)^2$. Division of the spring constant by A_f^j produces the modulus of subgrade reaction for a single footing:

$$k_n^j = \frac{K_n^j}{A_f^j} \quad (4)$$

This value is used for the normal stiffness of the interfaces below the pillars, adjusted according to the ratio of the base area of the footing over the cross-sectional area of the pillar at ground level. The settlement d_n^j of the foundation for a given normal force F_n^j is:

$$d_n^j = \frac{F_n^j}{K_n^j} \quad (5)$$

The value for the shear stiffness of the interface is calculated by the expression:

$$k_s^j = \frac{k_n^j}{2(1+\nu)} \quad (6)$$

according to the Poisson's ratio ν of the stone masonry foundation. This value is not determined experimentally but is consistent with the material properties of the stone masonry and is numerically more stable and less arbitrary than the use of a dummy value that precludes shear slipping at the foundation. This slipping

mode is, in any case, constrained by the high compressive stress applied on the interface by the self-weight and the lack of horizontal loads. Therefore, the shear stiffness is calculated for a Poisson's ratio of 0.20 without further investigation.

The soil beneath the church foundations has been investigated and found to be generally composed of, from the surface advancing in depth: a) sandy clay (± 2.0 m thick), b) highly compressible peat (± 2.0 m thick), c) sandy clay (± 2.6 m thick), d) quaternary clay-containing sand (± 5.4 m thick) and e) tertiary highly consolidated clay-containing sand (unknown thickness) [10]. The foundation bases of the main pillars are roughly in the middle of the peat layer. In the present case study, the settlements have been calculated prior to this investigation. Therefore, the interface normal stiffnesses can be directly calculated from eq. (5) and (4). Using eq. (3) the apparent Young's modulus of the homogenized foundation soil can be back-calculated. In the case of the nave pillars at the final settlement (as shown in Figure 4) this apparent Young's modulus is equal to $0.597\ N/mm^2$ or $2.400\ N/mm^2$ when taking into account or disregarding the effect of embedment respectively. The former value is representative of peats, while the latter is rather low for the all the soils in the other layers. This indicates the major contribution of the peat layer to the total settlements and the potential primary cause of the excessive settlements of the church at the nave.

For all analysis cases, the structure is let to deform under its self-weight and the extra load applied at various levels of the nave wall from other elements present in the structure but not explicitly modeled, such as the timber roof or the stone masonry vaults.

All finite element calculations were carried out using the DIANA FEA package [22]. The geometric layout and the boundary conditions applied are illustrated in Figure 7. The different phases are colored in shades of grey and the areas where pillar masonry material is assigned are given a reddish overlay. It is assumed that the tower to the west of the nave (left side in the illustration) provides a rigid lateral support to the nave. This assumption is based on the greater bending stiffness of the tower, due to greater foundation depth, better preservation state, wall thickness and closed box plan, compared to that of the nave wall. It is further assumed that the nave wall is not constrained towards the crossing in the east. This assumption, in turn, is based on the connection to the transept

being effected by the vaults, which cannot provide significant constraint to a solid masonry wall. The average element length is roughly 166 mm, resulting in a total of 40308 nodes and 13029 continuum and 37 interface elements. The roof loads associated with each of the three phases is applied at the top of every model.

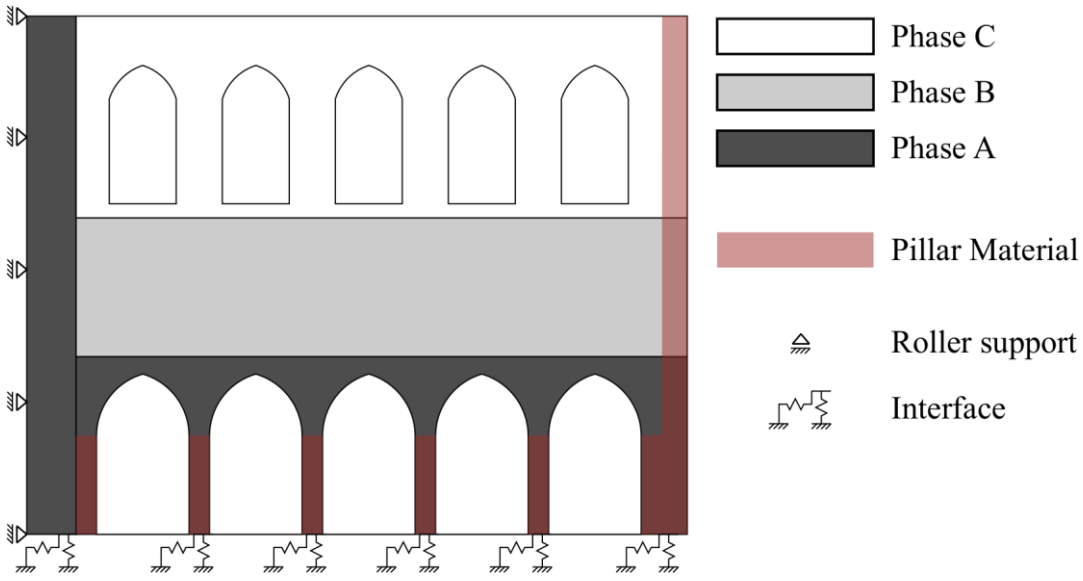

Figure 7 Geometric layout of church nave wall. Structural phase designation, boundary conditions and material assignment.

3.3 Definition of Time Periods for Phased Analysis

Three different time periods are defined for the investigation of the time-dependent behavior of the building: period A (1300-1316), period B (1317-1534) and period C (1535-1970), which coincide with the construction phases illustrated in Figure 7. The beginning of period A corresponds to the completion of the first nave wall level. The end of period A corresponds to the initiation of the increase of the height of the nave and period B starts upon its completion. The end of period B corresponds to the construction of the crossing and the third level of the nave wall. Period C brings us near to the present period, at the time of major temporary shoring of the building. The analysis period covers the entire history of the monument up to before the point of internal shoring. The post-intervention state of the monument will be a subject of further study in the future.

Through use of the equations (3) to (5), and for known values of the applied force and displacement, one may calculate the normal interface stiffness, and also back-calculate the apparent Young's modulus of the soil at given time instants. Both the forces and the settlements have been estimated for various points in the history of the building, as shown in Figure 4. The calculated normal interface stiffness for different structural parts through time is shown in Figure 8. This value is proportional to the apparent Young's modulus of the soil. One can differentiate between a short-term Young's modulus, governed by immediate settlements due to a change in load, and a long-term Young's modulus, governed by settlements due to, for example, consolidation. In the case of the pillars, the short-term Young's modulus generally exhibits a decreasing trend, whereas the long-term modulus exhibits an increase. The two curves appear to converge near the end of the measurement period, indicating that processes causing settlement under sustained loads have been halted. The consolidation being further completed accounts for the latter phenomenon, but the continuation of the settlements cannot be entirely excluded.

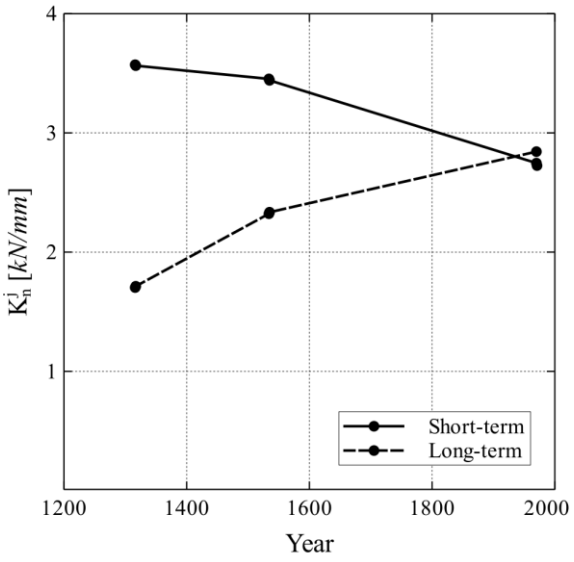

Figure 8 Calculated pillar spring stiffness for estimated loads and settlements. Development of instant and long-term response.

3.4 Analysis Approaches

Three different approaches will be adopted for the analysis of the nave: a single-phase analysis, a phased analysis and a parametric study.

Firstly, in the single-phase analysis, the whole structure is taken in its entirety and the foundation interfaces are assigned their final values according to the estimated settlements of each structural part and the dimensions of the footings.

Secondly, in the phased analysis, three major phases are considered, with each one decomposed into two parts. The major phases correspond to the phase designation indicated in Figure 7 and the decomposition of each phase is based on the differences between the short-term (immediate) and the long-term response of the structure under the sustained loads of each phase. Both the single-phase analysis and phased analysis make use of approach (b) for determining the interface normal stiffness as explained in Section 3.2. In order to facilitate the conformity of the previously and newly active parts of the mesh during the transition between phases, the structure was unloaded in a stepwise manner before the activation of the new parts. This approach maintains the damage location and the local reduction of stiffness due to cracking.

The self-weight is applied in 50 steps for each phase of all the analyses. A regular Newton-Raphson iteration method is employed, with a 0.001 energy norm for convergence. Thirdly, a parametric analysis is performed to address uncertainties in the mechanical properties of the materials. In order to reduce the computational cost, these analyses are only carried out for the settlement profile obtained from the levelling surveys of the period 1994-2005. Such analysis is defined in Section 3.2 as approach (a) for determining the normal stiffness. In the following section, this choice of loading is motivated further, through a discussion of the obtained failure patterns. The material parameters included in the investigation are the Young's modulus, the tensile strength and the tensile fracture energy of the masonry composing the nave. The variation of the parameters ranged from 50% to 200% of the initial values indicated in Table 1. The model using the initial values will be henceforth referred to as the reference model.

4. Analysis Results

4.1 Single-Phase Analysis

As a first approach, the self-weight of the complete structure along with the final additional roof weights is applied in a single phase. The final value for the stiffness of the foundation interfaces is used (see Figure 8), corresponding to the long-term soil modulus of phase C. The obtained crack pattern is shown in Figure 9. The obtained damage pattern presents several differences from the actual structure. Due to the settlement towards the crossing, the response is dominated by the separation cracks between the nave and the tower. Crack 2 above arch 2 (Figure 2) is entirely absent. A single crack is formed between pillars 2 and 3 (crack 3, but inclined in the other direction) and the crossing itself remains intact, as does its connection with the wall. Therefore, application of the deformation loads in a single analysis step reveals only part of the response of the building and is not indicative of its behavior throughout its history.

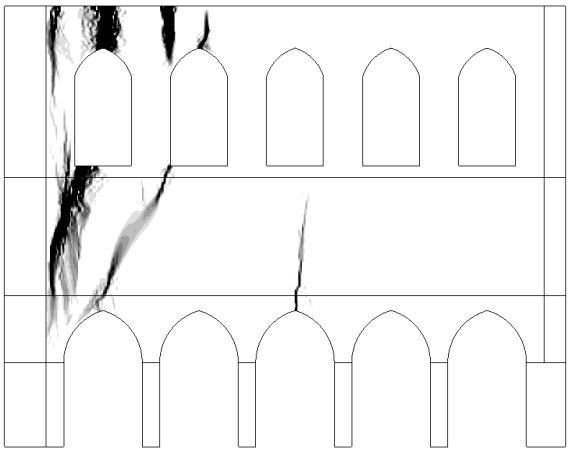

Figure 9 Crack patterns for application of load in single analysis phase.

4.2 Phased Analysis

The phased analysis of the nave provides a much more complete and detailed illustration of the development of damage on the building throughout its history (Figure 10). The obtained settlement profiles derived from the phased analysis, as well as from the single-phase case, are presented in Figure 11.

During phase A, only slight damage is registered at arches 1 and 5, see Figure 10a. There is some widening of the cracks under long-term loading, but no formation of new major cracks, see Figure 10b. The response is mostly of a sagging type due to the tower and the crossing exhibiting only minor settlement. Due to the numerical cracks not having sufficiently developed in extent, no clear comparison between the numerically derived cracks and the existing damage in the building can be made.

The situation changes significantly during phase B with the increase of the height of the nave wall above the colonnade. A major separation crack is formed in the short-term phase between the tower and the nave (cracks 1 and 5). Additionally, cracks 2 and 3 are formed above pillar 3. At the end of the long-term loading, cracks 1 and 4 have emerged above the main colonnade. While the settlement profile is mostly of a sagging type at the end of the short-term phase (Figure 11), a mixed profile with a significant tilting component is obtained at the end of the long-term phase. The increase of the weight at the crossing is substantial and unable to be borne by its foundations.

Phase C witnesses the formation of the new cracks above and beside the third level windows (cracks 6 and 7 in Figure 2). The extent of the previously formed cracks is increased without, however, significant widening, indicating the activation of the cracks at the new parts of the structure. As shown in Figure 11, the obtained profile resembles the tilting-dominated response at the end of phase B, but of a larger magnitude.

In Figure 11, the maximum settlement obtained at the end of the phase C closely resembles that of the single-phase analysis, albeit with a slightly smaller magnitude. Nevertheless, the cracking pattern is significantly different in the two approaches. The resulting cracking pattern from the phased analysis resembles in a higher degree the actual pattern (compare Figure 2 and Figure 10). The cracking pattern resulting from the phased analysis resembles much more closely the actual crack pattern compared to the single-phase analysis (compare Figure 9 and Figure 10). The complexity of the model, as the outcome of soil-structure interaction, is underlined by the substantially different settlements obtained between the four pillars. This is despite the fact that they are of the same cross-section with identical foundations (meaning equal interface stiffness) and bearing roughly the same vertical loads.

Overall, as time progresses, the deflection ratio of the structure tends to decrease, despite the increase in the overall settlements (Figure 11). Cracks 2 and 3, caused by the sagging of the center are nearly fully developed by the end of phase B, after which newly arising damage is possibly associated with tilting of the nave towards the crossing. The maximum width of the cracks in the first level of the wall in fact decreases from phase B to phase C due to the stabilizing effect of the added stiffness of the second level and despite the increase in weight.

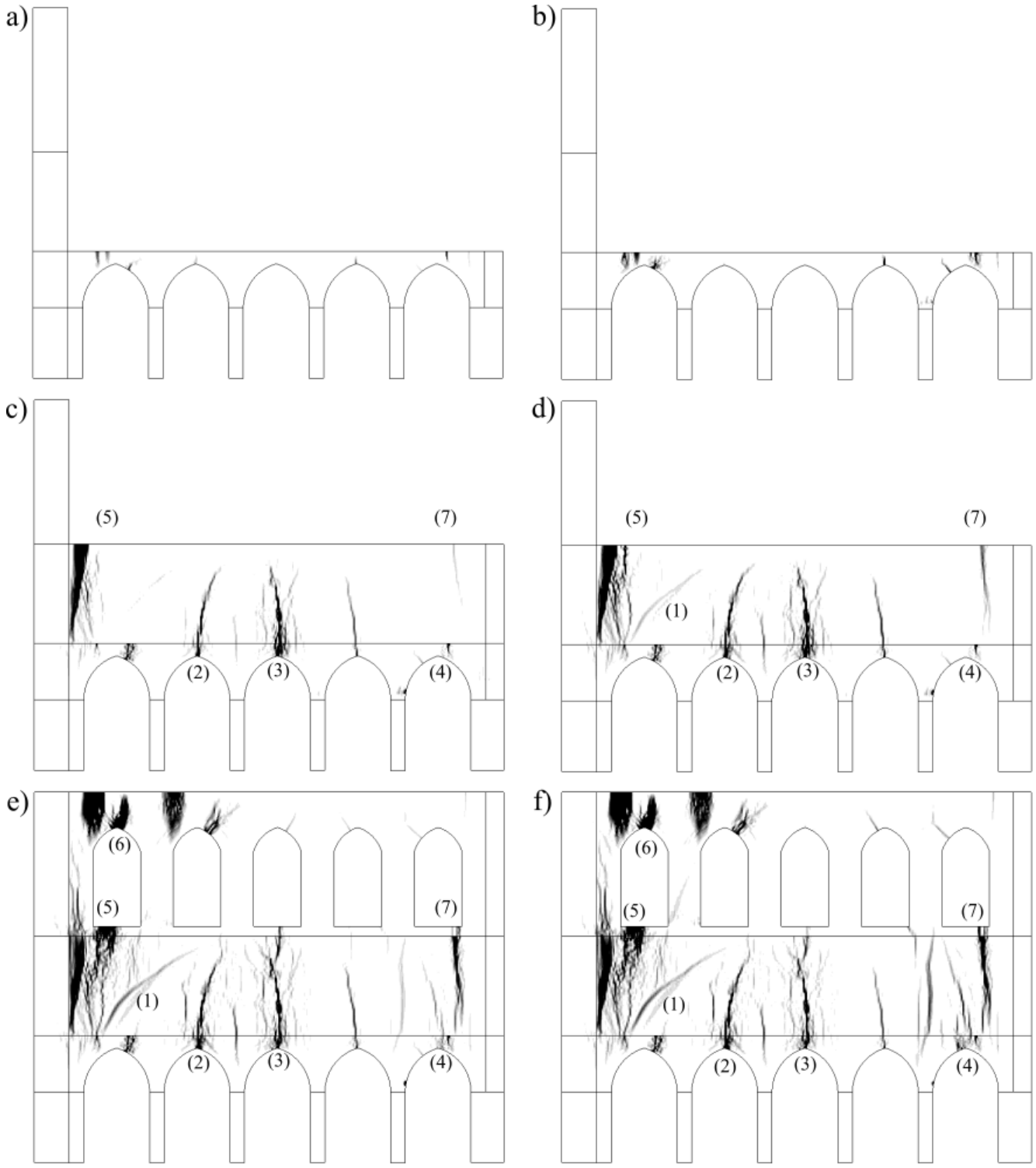

411

412 **Figure 10 Crack patterns for phased analysis of nave: a) phase A short-term, b) phase A long-term, c)**

413 **phase B short-term, d) phase B long-term, e) phase C short-term, f) phase C long-term.**

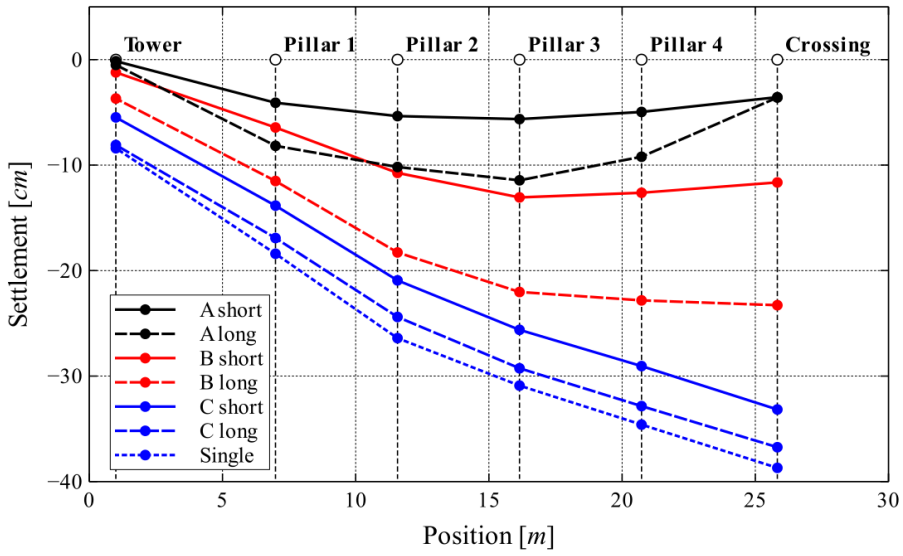

Figure 11 Settlement profiles obtained from finite element analysis: phased analysis and single-phase approaches.

The numerically obtained cracks have been linked to cracks documented in the structure (Figure 2 and Figure 10). Rather than integrating the obtained crack strains over the continuum to calculate the crack width, the opening of the cracks is indirectly calculated through measurement of the horizontal relative displacements of nodes on either side of the smeared crack mouth. Displacements due to elastic stress are minimal compared to displacements due to crack opening. In cases where the cracks in the actual structure are composed of more than one distinct branch, this measured numerical crack width is divided by the number of branches in order to obtain the magnitude of a single crack branch. The development of the normalized crack width, defined as the sum of the crack width divided by the number of crack branches in the actual structure, is presented in Figure 12. All cracks tend to increase with the passage of time, except crack 3, which is reduced in width after the construction of the second and third level of the nave.

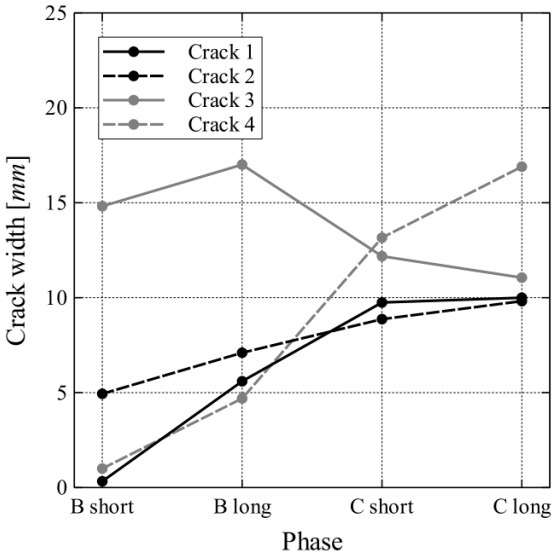

Figure 12 Normalized crack width for various analysis phases.

4.3 Parametric Investigation

The damage pattern obtained from the reference model is shown in Figure 13. This is the outcome of the application of the settlement pattern measured in the period 1994-2005. Rather than the displacement being applied to the supports directly, the stiffness of the interfaces was calibrated in order to match this settlement profile. This approach allows the evaluation of the soil-structure-interaction by altering the settlements from a variation of the stiffness of the superstructure.

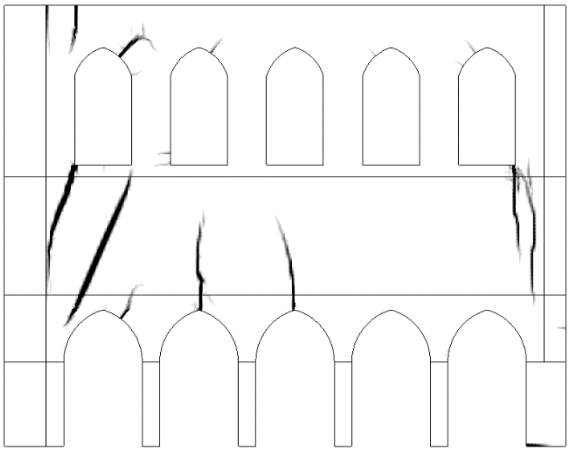

Figure 13 Crack pattern obtained from the reference model of the parametric investigation.

Despite the narrow extent of this measurement period compared to the entire history of the building, the pattern closely resembles the damage present in the structure, both in location and extent, albeit with a much smaller magnitude in terms of crack width. This constitutes an indication that the emergency measures taken from 1965 onwards may have not completely halted the progress of settlement in the structure. Nevertheless, this resemblance motivates the use of this measured profile as a basis in the parametric investigation carried out in this section.

The results of the parametric investigation are illustrated in Figure 14. They are presented in terms of the width of cracks 2 and 3 vs. settlement of pillar 2, above which the cracks in question are situated. Initially, the Young's modulus of the pillar was investigated, due to the initially determined value being higher than expected given the compressive strength of the pillar masonry (see Table 1). The change in the Young's modulus of the pillar does not significantly affect the response of the nave, due to the limited extent of the nave area in which it is encountered. However, the reduction of the Young's modulus of the wall increases both the width of the cracks and the amount of settlement of pillar 2. Interestingly, the reduction of the Young's modulus causes crack 2 to increase in width and crack 3 to be severely reduced, owing to the redistribution of forces in the wall. Cracks 2 and 3 are differently affected by changes in the tensile strength of the wall masonry as well. The width of crack 2 slightly increases for any change in the parameter, while crack 3 decreases, practically disappearing for a decrease in the tensile strength. Finally, the response was not particularly sensitive to changes in the tensile fracture energy of the wall masonry. However, a slight increase in the total settlement of the pillar is registered for a decreased value of this parameter.

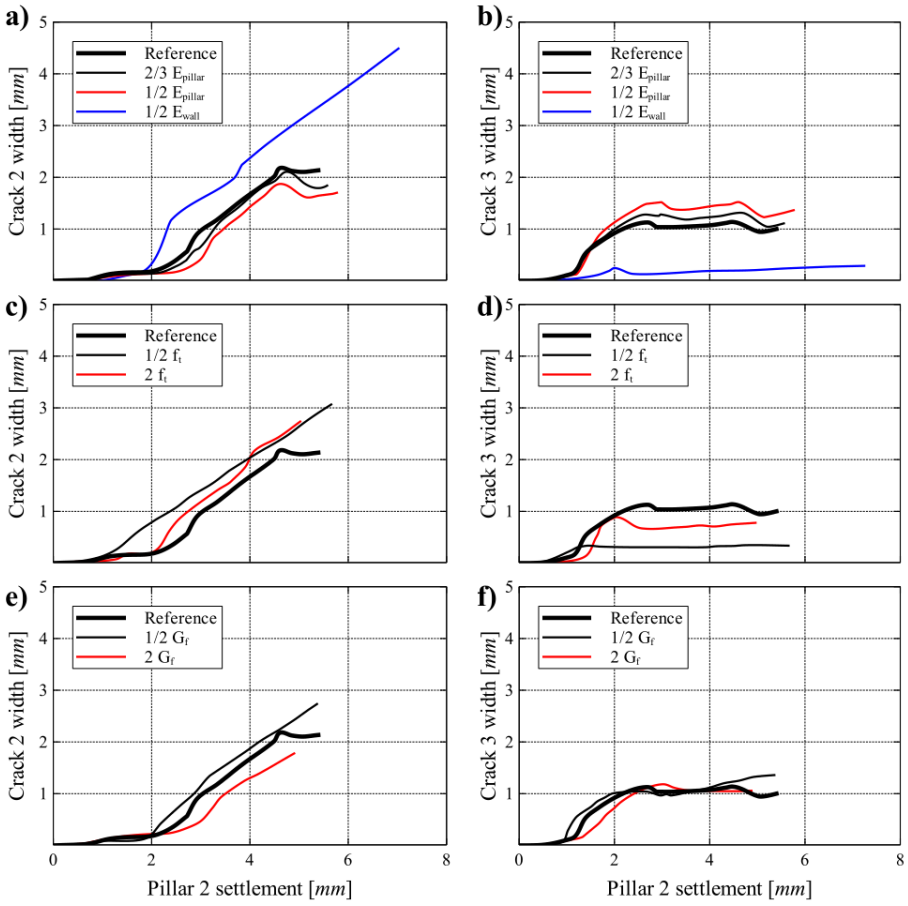

455

456 **Figure 14 Results of parametric investigation: a) & b) Crack width for variation of Young's modulus,**
457 **c) & d) crack width for variation of tensile strength, e) & f) crack width for variation of tensile fracture**
458 **energy.**

459 The results are also tabulated in Table 2, with the addition of the results of the horizontal movement and
460 vertical settlement of pillar 2. The changes in the horizontal movement of the pillar, measured at the capital and
461 indicating tilting rather than whole body slipping, are either associated with the crack widths above the pillar or
462 with the capacity of the wall for post-cracking deformation (as influenced by an increase in the fracture energy).

463 Crack 2 did not present strong sensitivity to the material properties. Crack 3 presented some sensitivity to the
464 tensile strength of masonry. The dependence on the Young's modulus of masonry is partially related to the increase
465 of crack width due to reduced stiffness of the superstructure. The tensile fracture energy had only a marginal effect
466 on either crack. The crack arrangement was not sensitive to the material properties. These observations suggest

that crack formation and development are more sensitive to the applied deformation profile. This outcome illustrates the importance of an accurate calculation of the properties of the soil and a good measurement of the historic settlement profile in order to achieve meaningful analysis results. In light of the envisaged intervention project, consolidation of the wall masonry, which would lead to some degree of increase of the tensile strength, fracture energy and Young's modulus of the material, can be beneficial in itself for maintaining the integrity of the church and limiting the effects of possible future differential settlement. This can act as a complement to the foundation strengthening and soil consolidation underway.

Table 2 Results of parametric investigation. Percentile differences from reference model results in crack width and displacement (vertical and horizontal) of pillar 2.

	Crack width 2	Crack width 3	$\Delta x_{pillar\ 2}$	$\Delta y_{pillar\ 2}$
Reference	100	100	100	100
$1/2\ f_t$	146	32	190	105
$2 f_t$	129	77	85	93
$1/2\ G_f$	129	137	76	99
$2 G_f$	83	105	271	91
$2/3\ E_{pillar}$	85	111	97	103
$1/2\ E_{pillar}$	80	136	102	107
$1/2\ E_{wall}$	218	29	352	134

4.4 Discussion on Model Results

A final appraisal of the obtained results from the modeling approaches is warranted. In particular, the results from the phased analysis need to be contrasted with the monitoring and survey data. The final deformation profile obtained for the phased analysis (Figure 11) relies on the estimation of the behavior of the soil through time. The profile estimated from the architectural features of the building (Figure 6) depicts the effects of soil-structure interaction more directly. The latter profile compares favorably with the deformation profile obtained from monitoring data over the period 1994-2005. The normalization of the estimated settlements by disregarding the tower movement prior to the construction of the nave wall makes a direct comparison difficult. The lack of measurements in the period 2005-2018 further complicates matters, which the new intervention project will help clarify. Finally, the analysis approach does not take into account the full three-dimensional geometry effects of the

structure. These are potentially more acute near the crossing pillar due to the presence of the transept. Nevertheless, the numerical analysis approach adopted here is able to capture the response of the nave with significant fidelity.

The assumption of a uniform interface stiffness below all the pillars in the nave is a necessary simplification due to the lack of more detailed data. Despite resulting in an accurate crack pattern, the final disposition is not in complete agreement with the settlement as estimated from the architectural feature analysis. However, a clearer relation between the numerical and measured deformation profile is obtained when comparing deflection ratios. The deflection ratio is defined as the ratio of the relative settlement to the length of the deflected part. In Figure 15, the deflection ratios along feature Line 4 (base of the pillar abacus of the first level) are presented, based on the measurements shown in Figure 6. The deflection ratio along this line could be more clearly defined along a larger portion of the structure compared to other lines and is sufficiently close to the base of the pillars to provide an indication of the settlement. As Figure 15 illustrates, the deflection ratios between the two approaches are quite similar, with the sagging of the colonnade between the tower and the crossing pillar being clearly indicated.

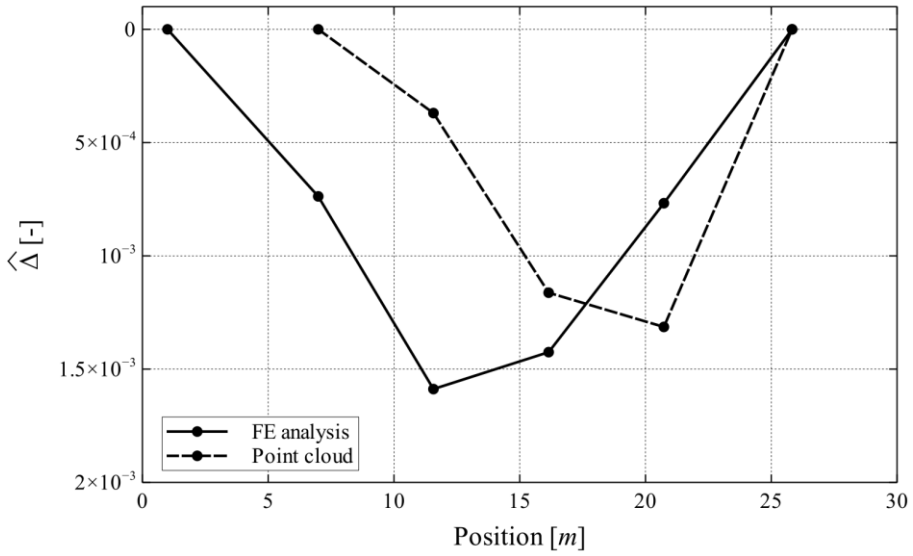

Figure 15 Comparison of deflection ratio from finite element analysis and architectural feature measurement on the point cloud (Line 4).

5. Damage Calculation Using an Analytical Damage Function

5.1 Calculation of Model Parameters

The model proposed by Giardina et al [7], which introduced an analytical relation between settlement and damage index for masonry buildings, will be adopted for the present study. The model relates the deflection ratio $\hat{\Delta}$ due to sagging or hogging ground deformation to a damage level of the structure according to the classification proposed by Burland & Wroth [23]. The damage level, linked to the severity of damage and the means required for its repair, is quantitatively expressed in terms of crack width, thus directly comparable to both documented pathology and nonlinear finite element analysis results. The damage classes are outlined in Table 3. The damage model for two-dimensional structures is a function of several geometric and material parameters expressed in a polynomial equation as follows:

$$d'_{2D}(\hat{\Delta}, \bar{\boldsymbol{x}}) = d_{2D,ref}(\hat{\Delta}) + \sum_{i=1}^{6} a_i \bar{x}_i = b_1 + b_2\hat{\Delta} + b_3\hat{\Delta}^2 + b_4\hat{\Delta}^3 + \sum_{i=1}^{6} a_i \bar{x}_i \quad (7)$$

where $d_{2D,ref}$ are the selected reference values, a_i and b_i are fitted polynomial coefficients and $\bar{\boldsymbol{x}}$ contains the normalized values of the model parameters x_i. The x_i model parameters, along with their reference values $x_{i,ref}$ are given in Table 4. All values for the polynomial coefficients and the normalization process for the model parameters are detailed in [7]. From the value of the damage level calculated from the model, one can calculate the corresponding crack width through linear interpolation based on the values found in Table 3.

Table 3 Damage classification for masonry structures subjected to differential settlements [23]**.**

Damage Level	Damage Class	Crack Width $[mm]$
1	Negligible	0.0 – 0.1
2	Very Slight	0.1 – 1.0
3	Slight	1.0 – 5.0
4	Moderate	5.0 – 15.0
5	Severe	15.0 – 25.0
6	Very Severe	>25.0

Table 4 Damage model reference values $x_{i,ref}$ [7] **and input for current analysis x_i.**

Openings	G_f	E	f_t	k_n	Interface shear behavior/Trough shape
$[\%]$	$[N/m]$	$[N/mm^2]$	$[N/mm^2]$	$[N/mm^3]$	$[-]$
$x_{1,ref} = 30$	$x_{2,ref} = 10$	$x_{3,ref} = 3000$	$x_{4,ref} = 0.10$	$x_{5,ref} = 0.7 \times 10^9$	$x_{6,ref} = 1$
$x_1 = 31.92 \div 33.88$	$x_2 = 12$	$x_3 = 3000$	$x_4 = 0.10$	x_5 = [See Table 5]	$x_6 = 1$

Parameters x_1 to x_4 are derived according to the material properties used in the finite element analysis and the geometry of the nave. Parameter x_6 is assigned its reference value according to [7]. Special attention is drawn to the parameter x_5 related to the normal stiffness of the soil-structure interface. The reference value for x_5 has been calculated according to typical Dutch pile foundation systems distributed along the façade of brick masonry structures [24]. In the present research, this parameter is calculated from the modulus of subgrade reaction under vertical loading of the foundation system of the nave, an approach that generalizes the applicability of the damage function to other foundation and soil types. This approach additionally allows for taking into account foundation strengthening, micro-piling and foundation soil improvement directly in the damage function.

For strip foundations, the modulus of subgrade reaction k_n is directly equivalent to the parameter x_5 and can be applied to continuous shallow foundations of masonry walls. Equations for its calculation are available in the literature (e.g. [25,26]). Some further manipulation is required in the case of colonnades founded on individual footings, as is the case with the nave pillars of the present case study. The x_5 parameter for a series of m single footings j is then calculated as follows:

$$k_n = \frac{\sum_{j=1}^{m} k_n^j A_f^j}{\sum_{j=1}^{m} A_f^j} = x_5 \tag{8}$$

where k_n^j is the modulus of subgrade reaction of footing j. This can be calculated from equations (3) and (4) or from equations (4) and (5) if the settlement has been pre-estimated. This averaging approach to the subgrade reaction modulus is similar to the one followed for the allocation of the stiffness provided by the distributed piles according to Rots [24], but can be generalized as shown for continuous footings of walls or isolated footings of colonnades. This parameter becomes significant in light of the results shown in Figure 11. Despite the decrease in the deflection ratio as the phases progress, the damage, in terms of crack width, increases. This is captured by the damage model through the change in the x_5 parameter due to soil-structure interaction (decrease of the apparent Young's modulus of the foundation soil within a single phase). The disposition of the data points, capable of being approximated by a third order polynomial fit, suggests that the damage model can be successfully adapted to this case.

In addition to adjusting the reference value for the vertical interface stiffness (x_5), the a_5 coefficient associated with the interface stiffness is also adapted. These parameters are modified in order to fit the available numerical results of the phased analysis (phase B and C) and the reference model. The material properties of masonry are taken as equal to those of the wall masonry (Table 1), which comprises most of the structure and on which the majority of the damage is accumulated. The percentage of openings varies between 33.88% in phase B and 31.92% in phase C and the reference model.

5.2 Results

Using equation (8) the values for the parameter x_5 are found for the colonnade. These are shown in Table 5, where it becomes apparent that the range of the parameter values varies within the range initially investigated in [7], with the exception of the reference model case. Nevertheless, it is expected that the calibrated values for the numerical model parameters be significantly different from those initially proposed. This is due to the fact that the initial model was calibrated against a finite element benchmark where the interface stiffness was not extensively investigated. A complete recalibration of the model is bound to alter the numerical parameters to some degree.

The slight increase of x_5 during the transition from long-term phase B to short-term phase C is contrary to the progress of soil consolidation, which decreases the apparent short-term Young's modulus of the soil. However, depending on the calculation method elected (such as for the estimated settlement method employed here or for continuous footings), the x_5 parameter may depend directly or indirectly on the stiffness of the superstructure as well. This stiffness is increased by the addition of the second level of the nave wall. This fact clearly illustrates the significance of soil-structure interaction in the study of differential settlement damage problems.

The analytical model, when used with its initial reference values and normalization process, greatly exaggerates the damage corresponding to the reference model and underestimates the damage in the phased analysis (phases B and C). The calibration of the new parameters is performed by a simple minimization process, during which the linear regression between FE and analytical crack widths is required to be a unitary slope curve. The normalization of the x_5 parameter in [7] is carried out according to:

$$\overline{x_5} = \frac{\log_{10} x_5 - \log_{10} x_{5,ref}}{2} \tag{9}$$

A new normalization of the parameters is proposed here in order to match the trend of interface stiffness to damage level, according to which the $\overline{x_5}$ parameter is equal to:

$$\overline{x_5} = \left(\frac{\log_{10} x_{5,ref}}{\log_{10} x_5} \right)^{1.5} \tag{10}$$

The results of the modified analytical model are compared with the finite element analysis results in terms of the main cracks of the first level of the nave wall, following their calculation as described in the phased analysis section. The minimization process for the available data set produces a value for the a_5 parameter equal to -1.1722. The comparison of the results is plotted in Figure 16a, in which satisfactory agreement is found throughout the range of available data. Despite some discrepancy in the results in terms of crack width, the damage level is well approximated by the calibrated model.

Table 5 x_5 parameter results for phase B model, phase C model and reference model.

		Reference	B short	B long	C short	C long
x_5	$[N/mm^3]$	1.43E+10	2.79E+07	9.63E+06	9.70E+06	6.86E+06

The envelope indicating the change in the polynomial model curve, almost entirely due to alterations in the spring stiffness and to a very minor extent due to changes in the opening percentage, is presented in Figure 16b. The upper envelope curve corresponds to the maximum apparent stiffness associated with the reference model and the lower curve corresponds to the minimum apparent stiffness of the long-term part of phase C. This fact illustrates the influence of the foundation stiffness, and, by extension, the properties of the soil, on the behavior of complex structures.

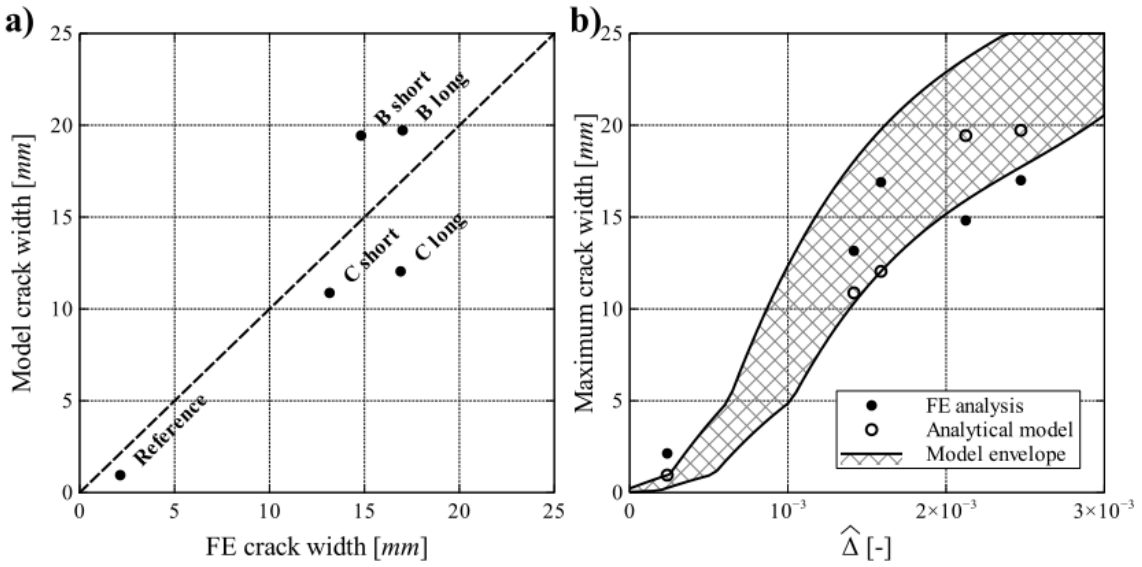

Figure 16 a) Comparison of analytical model with FE analysis results. Dashed diagonal indicates line of equality between FE analysis and analytical modeling. b) Crack width according to damage prediction model and comparison with FE analysis results.

The initial results of this approach towards the extension of the predictive analytical model are promising. The generalization of this extension requires robust verification in order to recalculate the numerical coefficients of the model. Coupled experimental tests and parametric numerical analyses need to be developed, along the same lines of the prior development of the analytical model but attempting to include variations in the vertical stiffness of the foundation. This is likely to lead to modifications to all numerical parameters, unlike the simplified calibration approach adopted in this paper, where only the parameters linked with the vertical stiffness were modified.

6. Conclusions

In this study the behavior of a church nave wall subjected to ground deformation over an extended period of time is investigated. The problem is approached through single-phase and multi-phase finite element analysis. The paper demonstrates the importance of detailed modeling of the soil behavior over time, the soil-structure interaction and the accurate measurement of settlements for the analysis of complex structures subjected to soil movement. Through this investigation it is shown that the application of a single-phase analysis does not reliably provide the cracking pattern observed in the actual structure. The need to take into account construction phases

and changes in the soil stiffness is clearly shown, even when studying individual element ensembles, such as the nave wall here investigated. The importance of detailed geometric and damage survey is also demonstrated.

The sensitivity analysis illustrates the predominance of the deformation profile, as influenced mainly by the soil-structure interaction, in the disposition of the cracking pattern on the structure. Nevertheless, the width of the cracks is strongly influenced by the material properties of the nave wall, as are the obtained settlements, although to a lesser degree.

The phased analysis, taking into account changes in the behavior of the soil and alterations in the geometry of the structure, provides a complete picture of the history of the nave's pathology. Different major cracks appear and develop at different phases of the building, due to redistribution of the forces and changes in the stiffness of the foundations.

An analytical model for the prediction of the damage level in masonry structures subjected to differential settlements is adapted and expanded. Moving beyond the initial formulation of the model, a method for the direct calculation of the normal stiffness of the structure is proposed. Following calibration of the numerical coefficients linked to this stiffness, the results of the model are consistent with the numerical analysis results and the crack state of the real structure. Further expansion of the model along the lines pursued here can greatly enhance the potential for accurate analytical modeling of complex masonry structures.

Acknowledgements

The authors acknowledge the funding received by BRAIN.be, Belspo in support of the GEPATAR research project ("GEotechnical and Patrimonial Archives Toolbox for ARchitectural conservation in Belgium" BR/132/A6/Gepatar).

References

[1] A.R. Sánchez, R. Meli, M.M. Chávez, Structural Monitoring of the Mexico City Cathedral (1990-2014), Int. J. Archit. Herit. 10 (2016) 254–268. doi:10.1080/15583058.2015.1113332.

[2] L. Giresini, Energy-based method for identifying vulnerable macro-elements in historic masonry churches, Bull. Earthq. Eng. 14 (2016) 919–942. doi:10.1007/s10518-015-9854-7.

[3] F. Portioli, L. Cascini, Large displacement analysis of dry-jointed masonry structures subjected to settlements using rigid block modelling, Eng. Struct. 148 (2017) 485–496. doi:10.1016/j.engstruct.2017.06.073.

[4] S. Galassi, G. Misseri, L. Rovero, G. Tempesta, Failure modes prediction of masonry voussoir arches on moving supports, Eng. Struct. 173 (2018) 706–717. doi:10.1016/j.engstruct.2018.07.015.

[5] P. Roca, M. Cervera, L. Pelà, R. Clemente, M. Chiumenti, Continuum FE models for the analysis of Mallorca Cathedral, Eng. Struct. 46 (2013) 653–670. doi:10.1016/j.engstruct.2012.08.005.

[6] S. Saloustros, L. Pelà, P. Roca, J. Portal, Numerical analysis of structural damage in the church of the Poblet Monastery, Eng. Fail. Anal. 48 (2015) 41–61. doi:10.1016/j.engfailanal.2014.10.015.

[7] G. Giardina, M. Hendriks, J.G. Rots, Damage Functions for the Vulnerability Assessment of Masonry Buildings Subjected to Tunneling, J. Struct. Eng. 141 (2015) 1–13. doi:10.1061/(ASCE)ST.1943-541X.0001162.

[8] D. Peduto, G. Nicodemo, J. Maccabiani, S. Ferlisi, Multi-scale analysis of settlement-induced building damage using damage surveys and DInSAR data: A case study in The Netherlands, Eng. Geol. 218 (2017) 117–133. doi:10.1016/j.enggeo.2016.12.018.

[9] D. Peduto, S. Ferlisi, G. Nicodemo, D. Reale, G. Pisciotta, G. Gullà, Empirical fragility and vulnerability curves for buildings exposed to slow-moving landslides at medium and large scales, Landslides. 14 (2017) 1993–2007. doi:10.1007/s10346-017-0826-7.

[10] L. Schueremans, K. Van Balen, K. Brosens, D. Van Gemert, P. Smars, The Church of Saint-James at Leuven: Structural Assessment and Consolidation Measures, Int. J. Archit. Herit. 1 (2007) 82–107.

643 doi:10.1080/15583050601126137.

644 [11] S. Sanchez-Beitia, L. Schueremans, K. Van Balen, On-site stress measurement on the piers of the Saint
645 Jacobs church in Leuven, Belgium, Int. J. Archit. Herit. 3 (2009) 110–125.
646 doi:10.1080/15583050802278794.

647 [12] E. Verstrynge, L. Schueremans, P. Smars, Controlled Intervention: Monitoring the Dismantlement and
648 Reconstruction of the Flying Buttresses of Two Gothic Churches, Int. J. Archit. Herit. 6 (2012) 689–708.

649 [13] G. Heirman, K. Brosens, Uitvoeringsdossier Globale Stabiliteitswerken Sint-Jacobskerk. Internal report
650 D/0800/10, Triconsult nv, 2017.

651 [14] M. Bassier, G. Hardy, L.-E. Bejarano-Urrego, A. Drougkas, E. Verstrynge, K. Van Balen, M. Vergauwen,
652 Semi-automated creation of accurate FEM meshes of heritage masonry walls from point cloud data, in:
653 11th Int. Conf. Struct. Anal. Hist. Constr. Cusco, Peru, 2019: pp. 305–314.

654 [15] K. Van Balen, K. Nuyts, P. Smars, D. Van de Vijver, Optimalisatie van standzekerheidsmodellen van
655 gewelfde gotische structuren gebruik makend van informatie uit vervormingsmetingen en scheuranalyse.
656 Internal report PV30318, KU Leuven, 1995.

657 [16] A.W. Koppejan, A formula combining the Terzaghi load compression relationship and the Buisman secular
658 time effect, in: Proc. 2nd Int. Conf. Soil Mech. Found. Eng., 1948: pp. 32–38.

659 [17] G. Giardina, A. V van de Graaf, M. Hendriks, J.G. Rots, A. Marini, Numerical analysis of a masonry façade
660 subject to tunnelling-induced settlements, Eng. Struct. 54 (2013) 234–247.
661 doi:10.1016/j.engstruct.2013.03.055.

662 [18] A. Drougkas, P. Roca, C. Molins, Numerical prediction of the behavior, strength and elasticity of masonry
663 in compression, Eng. Struct. 90 (2015) 15–28. doi:10.1016/j.engstruct.2015.02.011.

664 [19] R. De Borst, Smeared cracking, plasticity, creep, and thermal loading—A unified approach, Comput.

Methods Appl. Mech. Eng. 62 (1987) 89–110.

[20] H.W. Reinhardt, Fracture Mechanics of an Elastic Softening Material Like Concrete., Heron. 29 (1984) 1–42. doi:10.1023/A:1012235530463.

[21] G. Gazetas, Foundation Vibrations, in: H.-Y. Fang (Ed.), Found. Eng. Handb., 1991: pp. 553–593. doi:10.1007/978-1-4615-3928-5_15.

[22] TNO, DIANA Finite Element Analysis, User's Manual, (2017).

[23] J.B. Burland, C.P. Wroth, Settlement of buildings and associated damage, in: Settl. Struct. Proc. Conf. Br. Geotech. Soc., 1974: pp. 611–764.

[24] J.G. Rots, Settlement Damage Predictions For Masonry, in: Maint. Restrengthening Mater. Struct. Brick Brickwork Proc. Int. Work. Urban Herit. Build. Maint. IV, 2000: pp. 47–62.

[25] M.A. Biot, Bending of an infinite beam on an elastic foundation, J. Appl. Math. Mech. 2 (1937) 165–184. doi:10.1016/0021-8928(58)90136-9.

[26] A.B. Vesić, Beams on Elastic Subgrade and the Winkler's Hypothesis, in: Proc. 5th Int. Conf. Soil Mech. Found. Eng. Paris, Fr., 1961: pp. 845–850.